ACS APPLIED MATERIALS & INTERFACES

Research Article

www.acsami.org

Avoiding Resistance Limitations in High-Performance Transparent Supercapacitor Electrodes Based on Large-Area, High-Conductivity PEDOT:PSS Films

Thomas M. Higgins and Jonathan N. Coleman*

School of Physics, CRANN and AMBER Research Centres, Trinity College Dublin, Dublin 2, Ireland

Supporting Information

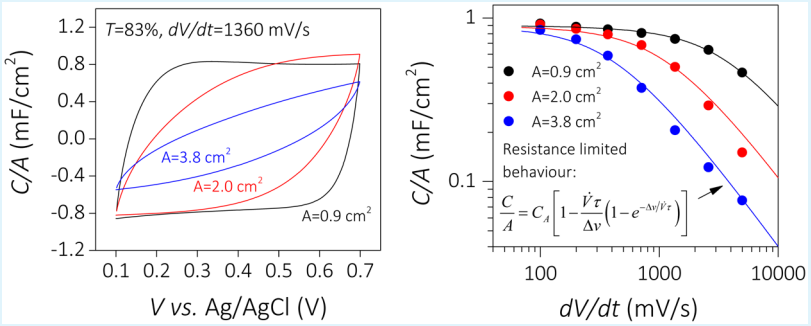

ABSTRACT: This work describes the potential of thin, spray-deposited, large-area poly(3,4-ethylenedioxythiophene)/poly(styrene-4-sulfonate) (PEDOT:PSS) conducting polymer films for use as transparent supercapacitor electrodes. To facilitate this, we provide a detailed explanation of the factors limiting the performance of such electrodes. These films have a very low optical conductivity of σ_{op} = 24 S/cm (at 550 nm), crucial for this application, and a reasonable volumetric capacitance of C_V = 41 F/cm^3. Secondary doping with formic acid gives these films a DC conductivity of σ_{DC} = 936 S/cm, allowing them to perform both as a transparent conductor/current collector and transparent supercapacitor electrode. Small-area films ($A \sim 1$ cm^2) display measured areal capacitance as high as 1 mF/cm^2, even for reasonably transparent electrodes ($T \sim 80\%$). However, in real devices, the absolute capacitance will be maximized by increasing the device area. As such, here, we measure the electrode performance as a function of its length and width. We find that the measured areal capacitance falls dramatically with scan rate and sample length but is independent of width. We show that this is because the measured areal capacitance is limited by the electrical resistance of the electrode. We have derived an equation for the measured areal capacitance as a function of scan rate and electrode lateral dimensions that fits the data extremely well up to scan rates of ~1000 mV/s (corresponding to charge/discharge times > 0.6 s). These results are self-consistent with independent analysis of the electrical and impedance properties of the electrodes. These results can be used to find limiting combinations of electrode length and scan rate, beyond which electrode performance falls dramatically. We use these insights to build large-area (~100 cm^2) supercapacitors using electrodes that are 95% transparent, providing a capacitance of ~12 mF (at 50 mV/s), significantly higher than that of any previously reported transparent supercapacitor.

KEYWORDS: *printed electronics, transparent electronics, conducting polymer, PEDOT:PSS, electrochemical capacitor, supercapacitor, percolation*

INTRODUCTION

Recently, exciting progress has being made toward the creation of electronic devices on everyday plastic substrates by liquid-phase processing techniques such as inkjet and aerosol-jet printing.[1−3] This approach is exciting, as it will enable devices to be produced with unusual characteristics, such as mechanically flexibility, stretchability, and even transparency.[3−5] It is likely that these possibilities will lead to numerous applications that are impossible using traditional manufacturing techniques.

In moving toward this goal, a wide range of transparent electrical device components have already been demonstrated. Examples include conducting elements and circuitry,[6,7] capacitors,[8] diodes,[9] transistors,[10] audio speakers,[11] and sensors for both chemical[12] and mechanical[13] stimuli. In addition to these energy-consuming components, transparent energy-harvesting systems are also under investigation to impart power generation capabilities, for example, using photovoltaic[14] and piezoelectric[15] technologies.

To mediate between these energy-harvesting and -consuming components, transparent energy storage systems must also be developed. As for traditional electronics, this role will most

Received: May 5, 2015
Accepted: July 15, 2015
Published: July 15, 2015

DOI: 10.1021/acsami.5b03882
ACS Appl. Mater. Interfaces 2015, 7, 16495−16506

likely be played by batteries and supercapacitors (SCs). While examples of the former are presently scarce,[16] significant efforts are underway to develop transparent/flexible SCs.[17−35] The electrode materials under investigation for this purpose are numerous, including carbon nanotubes,[27,32,33] graphene,[21,29,34] transition metal oxides,[17,19,20,23,25] and conducting polymers.[17,22,30]

In some transparent SC reports, the capacitive charge storage materials have been supported by an underlying transparent indium−tin oxide (ITO) layer to provide efficient current collection.[19−25] However, due to its brittle nature, the growing cost of indium, and the need for both high-vacuum and high-temperature processing,[36] it is unlikely this material will be compatible with future printed electronics. Rather, we believe it is more likely that future transparent/flexible SCs will contain ITO-free electrodes deposited directly on plastic substrates. Thus, developing an electrode material that can simultaneously provide excellent capacitive charge storage, efficient current collection, and high optical transparency is an important problem in this field.

With this being the case, here, we briefly outline some key physical relations and figures of merit relevant for characterizing the performance of transparent SC electrodes. As for any SC electrode, the primary measures of performance are the stored energy (E) and power output (P), given by

$$E = \frac{1}{2} C \Delta V^2 \tag{1}$$

$$P = \frac{1}{4} \frac{\Delta V^2}{R_{ESR}} \tag{2}$$

Although the electrode interfacial potential difference, ΔV, is clearly important, it is strongly influenced by the properties of the electrolyte (~1.2 V for devices that employ aqueous electrolytes). Most important from a materials standpoint are the electrode capacitance, C, and associated equivalent series resistance, R_{ESR}, which must be maximized and minimized, respectively. For this specific application, it is crucial to understand how both of these properties are related to the electrode transparency, T.

The capacitance that a given electrode is able to supply depends on its volumetric capacitance, C_V, and its dimensions. In practical terms, the areal capacitance, C_A, is the most relevant measure of capacitance in transparent/flexible devices when considering that multiple device components must be assembled onto a given area of substrate (e.g., hand-held devices, functional packaging, or e-labels). The areal and volumetric capacitance are related via $C_A = C_V t$, where t is the electrode thickness. As defined here, C_A and C_V are both rate-independent quantities and hence indicate the capacitance realized in the absence of transport limitations (these limitations will be discussed later). The C_A of a transparent electrode is related to its optical transmittance, T, via the expression[27]

$$T = \left(1 + \frac{Z_0 \sigma_{op}}{2 C_V} C_A\right)^{-2} \tag{3}$$

where Z_0 is a constant (377 ohm) and σ_{op} is the optical conductivity. This property is a measure of how much light the electrode material absorbs, and it is directly proportional to the Beer−Lambert absorption coefficient. Clearly, the ratio C_V/σ_{op} must be maximized to optimize the areal capacitance available for a given electrode transparency and thus it can be considered to be a figure of merit for transparent capacitive films (FoM_c). We emphasize that, unlike traditional SC electrodes, the gravimetric capacitance, C_M, is of little relevance when characterizing transparent SCs electrodes. This is because the mass of the electrode materials is insignificant compared with that of the plastic substrates supporting them. In addition, it is difficult to measure the mass of ultrathin films and therefore use of this metric inhibits the accurate comparison of different transparent supercapacitor materials.

Regarding the electrode equivalent series resistance, it is known that the R_{ESR} of transparent charge storage devices depends strongly on the electrical properties of the charge storage films, which, in this situation, must also act as current collectors.[27] To characterize this behavior, the electrode sheet resistance, R_s, can be related to T via a similar expression as that for the areal capacitance[37]

$$T = \left(1 + \frac{Z_0}{2R_s} \frac{\sigma_{op}}{\sigma_{DC}}\right)^{-2} \tag{4}$$

Here, σ_{DC} is the electrical conductivity of the thin film material. Thus, here, the ratio σ_{DC}/σ_{op} provides an electrical figure of merit (FoM_e) that must be maximized when optimizing the power output capabilities of transparent charge storage films.

In summary, although a thin film can have any desired transparency by making it sufficiently thin, doing so entails a corresponding increase in R_s, with implications for current collection and hence power. Moreover, high T simultaneously results in reduced C_A and, hence, a reduction in the energy that can be stored by a device with a given footprint.[27,32] Quantifying these trade-offs using the described figures of merit will greatly assist with the development of high-performance, transparent SCs.

In addition to these considerations, in this work, we identify a further property trade-off that is important for the design of transparent SCs: For a given electrode material (with some σ_{DC}, σ_{op}, and C_V), if the film thickness is constrained to maintain some desired transparency, then the only remaining option to attain larger absolute capacitance is by increasing the lateral dimensions of the electrodes. In doing so, C should scale linearly with film area (i.e., $C = C_A A$). However, for larger films, charge storage sites more distant from the external electrical contact will eventually become inaccessible, particularly when the film is charged and discharged quickly. Understanding such lateral dimension effects will be necessary for scaling-up device area for application in transparent electronics.

Here, we address this need by exploring the transparent SC properties of a sprayed conducting polymer, PEDOT:PSS, as a function of both film thickness and lateral dimensions. This commercially available conducting polymer has shown much potential to replace ITO within low-cost printed electronics applications such as organic solar cells[38−40] and organic light emitting diodes.[40] In addition, it is also being explored for use within both SC and battery electrodes.[41] As such, a detailed exploration of the potential of sprayed PEDOT:PSS for use within transparent/flexible energy storage applications is required.

RESULTS AND DISCUSSION

Optoelectronic Properties of Sprayed PEDOT:PSS Films. Aqueous solutions of PEDOT:PSS were deposited onto flexible plastic substrates (PET) to form thin films using a

DOI: 10.1021/acsami.5b03882
ACS Appl. Mater. Interfaces 2015, 7, 16495−16506

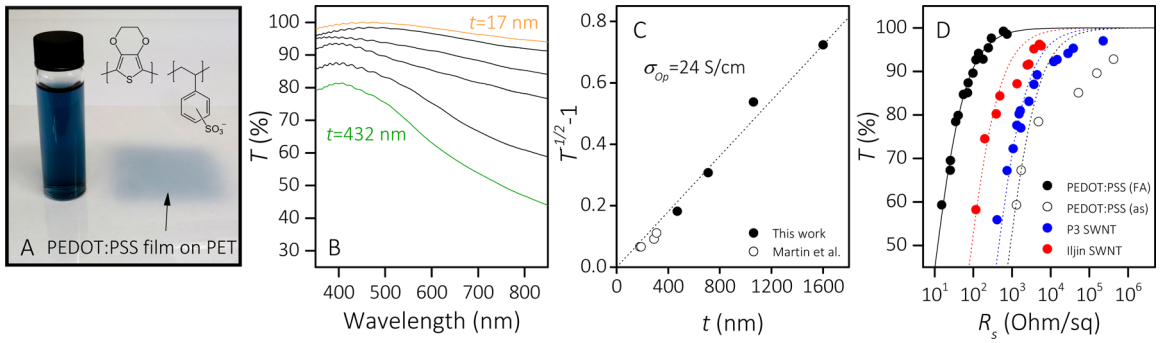

Figure 1. Characterization of the optoelectronic properties of sprayed PEDOT:PSS films. (A) Photograph of an aqueous PEDOT:PSS dispersion and a film (5 × 5 cm^2, T = 70%) on a PET plastic substrate. (B) UV−visible transmittance spectra of various sprayed PEDOT:PSS films. (C) Plot of $T^{-1/2} - 1$ (at 500 nm) vs film thickness, t, to determine the optical conductivity of PEDOT:PSS using eq 5. Unfilled points are spin-coated PEDOT:PSS films described by Martin et al.[43] (D) Film transmittance at 550 nm as a function of sheet resistance for the as-prepared PEDOT:PSS films (unfilled black circles), after treatment with FA (filled black circles), and data for disordered SWNT networks (P3 SWNTs and Iljin SWNTs). Fits to these data use eq 4.

robot-controlled airbrush spray system. Figure 1A presents a photograph of a characteristically blue aqueous PEDOT:PSS solution and a typical film produced (T = 70%). Although relatively small-area films were prepared for initial characterization (5 × 5 cm^2), this spraying system allows for films up to 18 × 18 cm^2 to be produced (Supporting Information, Figure S1). In principle, the stage area could be extended to produce arbitrarily large films. Details of the spray parameters employed in this work are given in the Supporting Information.

The film transmittance, T, was varied by altering the volume of PEDOT:PSS solution deposited onto the substrate. This was quantified by measuring UV−visible transmittance spectra, presented in Figure 1B. For conducting thin films, the transmittance for a given thickness, t, is controlled by the optical conductivity of the material, σ_{op}, via the equation[42]

$$T = [1 + Z_0\sigma_{op}t/2]^{-2} \quad (5)$$

Although use of this expression is not common within the transparent SC field, it is frequently employed by transparent conductor researchers.[37] We note that by expansion to first order, eq 5, is identical to the Lambert−Beer law ($T = e^{-\alpha t}$) with $Z_0\sigma_{op} \approx \alpha$, the optical absorption coefficient. The optical conductivity of PEDOT:PSS was determined by measuring the thickness of a number of sprayed films using profilometry, which found values between 470 and 1600 nm (note that these measurements were obtained after the formic acid secondary doping treatment described below for films that were sprayed onto glass substrates). By plotting this data as $T^{-1/2} - 1$ vs t (550 nm, Figure 1C) and fitting eq 5, we obtained a value of σ_{op} = 24 S/cm (at 550 nm) for these PEDOT:PSS films. For comparison, data for spin-coated PEDOT:PSS films described by Martin et al.[43] is included (unfilled points), falling close to our fitted curve. This value for σ_{op} is extremely low compared to that of other conducting materials: silver nanowires display values in the range 38−65 S/cm,[44,45] SWNTs have 150−200 S/cm,[46,47] and graphene has 100−2000 S/cm.[48] We believe this low optical conductivity of PEDOT:PSS will be critical to its success within transparent SCs (or conductors). Using σ_{op} = 24 S/cm with eq 5, the thickness of any PEDOT:PSS film can be determined from its transmittance spectrum. This is useful because it avoids difficulties associated with obtaining accurate thickness measurements of ultrathin films by physical methods such as atomic force microscopy. For the spectra shown in Figure 1B, t varied between 17 and 432 nm.

As for traditional SC electrodes, electronic transport to and from the electrochemical interface must occur efficiently to enable high-power device operation.[27,49] Accordingly, next, we characterized the electrical properties of these PEDOT:PSS films to evaluate their suitability to act as transparent electrodes without additional current collectors. Although the electrical conductivity of as-prepared PEDOT:PSS films are relatively poor, dramatic improvements are easily obtained by exposing the films to a variety of secondary dopants, such as sorbitol,[50] ethylene glycol,[36] dimethyl sulfoxide,[36] methanol,[51] and H_2SO_4.[52] Here, we have used the simple treatment reported by McCarthy et al.,[53] which involves dipping the PEDOT:PSS films in formic acid (FA) at room temperature for ∼5 s.

The effect of this treatment was evaluated using the four-point probe method. We calculated the R_s of these films before and after exposure to FA, which is plotted as a function of film transmittance in Figure 1D. Clearly, the treatment dramatically improved the electrical properties of these transparent films, consistent with previous reports.[53] At high transmittance (e.g., T = 90%), the sheet resistance is reduced by 3 orders of magnitude, falling from an untreated value of R_s = 1.5 × 10^5 ohm/sq to 102 ohm/sq after treatment. We note that the film with T = 90% and R_s = 102 ohm/sq represents exceptional performance for a transparent electrode of any sort.[37] Only silver nanowire networks routinely display better performance.[37,44] We can determine the ratio of DC to optical conductivities as a figure of merit (FoM$_e$) for transparent conductors by fitting eq 4 to the data in Figure 1D. For these PEDOT:PSS films, we find a value of σ_{DC}/σ_{op} = 39. For comparison, data for transparent current collectors formed by disordered networks of two different types of SWNTs are also shown: those characterized as transparent supercapacitors by King et al.[27] and Iljin SWNTs characterized in this work (see Supporting Information for SWNT network preparation). Fitting eq 4 to these data sets yields σ_{DC}/σ_{op} = 2 and 5, respectively, highlighting the excellent performance of these FA-treated PEDOT:PSS films. We note that the transmittance spectra were largely unchanged by the FA post-treatment (Supporting Information, Figure S2A), indicating that the increased σ_{DC} is responsible for the improved FoM$_e$ rather than it being due to substantial changes in σ_{op}.

As the optical conductivity is known, we can calculate the DC conductivity of the treated PEDOT:PSS films using the FoM$_e$ as σ_{DC} = 936 S/cm. This value is quite high for polymeric

DOI: 10.1021/acsami.5b03882
ACS Appl. Mater. Interfaces 2015, 7, 16495−16506

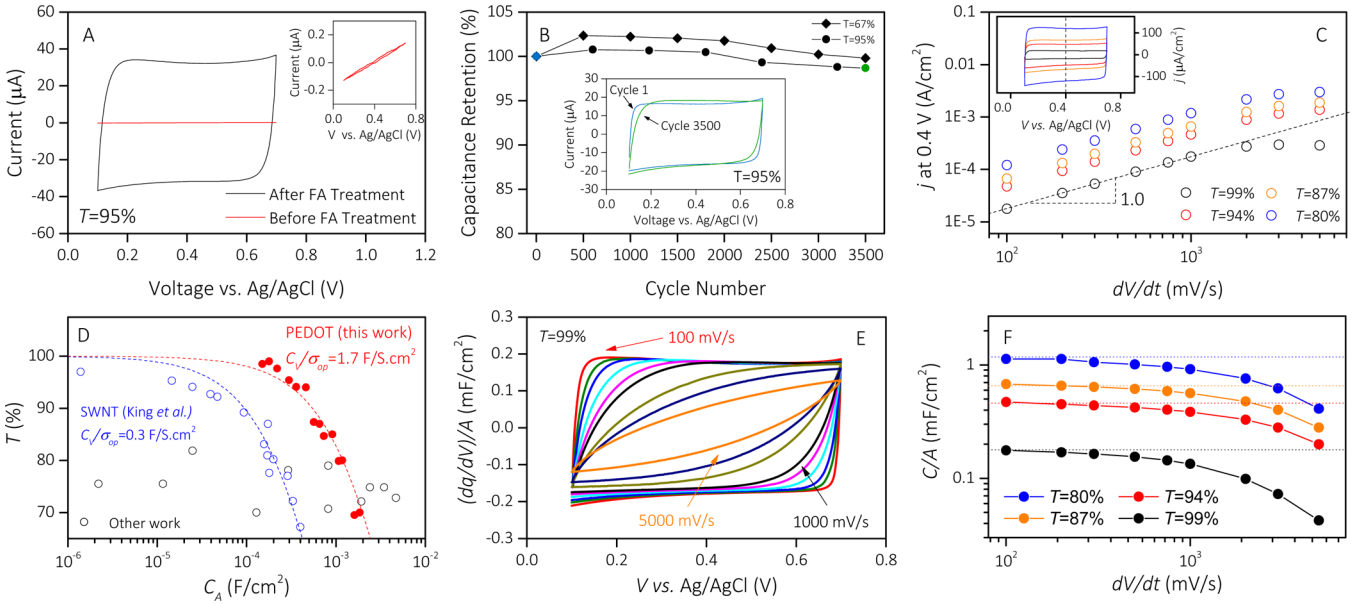

Figure 2. Characterization of the charge storage properties of small-area PEDOT:PSS films (L = 1 cm and W = 1 cm) by cyclic voltammetry. (A) CV response before (red) and after (black) FA treatment. (B) Capacitance retention of FA-treated films upon repeated cycling. Inset compares the CV response at cycles 1 and 3500 for a film with T = 95%. (C) Current density evaluated from CVs at 0.4 V vs Ag/AgCl for FA-treated samples at various scan rates. Ordinate intercepts enable extraction of the rate-independent areal capacitance, C_A. The (C) inset gives example CVs for four samples (dV/dt = 100 mV/s). (D) C_A plotted as a function of T, which includes a range of data taken from the literature (Supporting Information, Figure S4, contains a reproduction of this figure indicating sources of the literature data, not shown here for clarity). Dashed lines are fits to eq 3, with C_V/σ_{op} = 1.7 F/S·cm^2. (E) CVs for a single film (T = 99%) at various scan rates. Current density is reexpressed as a differential capacitance. (F) C/A found by integrating CV current over the potential window. Dashed lines indicate the C_A values obtained in (C).

conductors, albeit not as high as some other recent reports: PEDOT:PSS films have been demonstrated with a DC conductivity of 1418 S/cm when treated with ethylene glycol[36] and 3000 S/cm when treated with 1.5 M H_2SO_4 at 160 °C.[52] This value is competitive with the best data for carbon nanotube films[37] and significantly better than most solution-processed graphene electrodes.[54] Although a metal grid or mesh could be deposited on the film to further improve current collection, this would impair the electrode transmittance and complicate electrode processing. Rather, it would be preferrable that a single electrode material be used to provide sufficient electrical conductivity and high capacitive charge storage simultaneously.

Considering Figure 1D, for both the SWNT and untreated PEDOT:PSS data, there is marked deviation from the fits described by eq 4 at higher transmittance values. These deviations are more apparent by replotting the data as $T^{-1/2} - 1$ vs R_s, shown in Supporting Information, Figure S2B. Here, the linearized fits correspond to bulk-like behavior. Deviations from eq 4 have been explained as a manifestation of percolation-type phenomena.[55] While this is probably the case for the nanotube films, for the untreated PEDOT:PSS deviation from bulk-like behavior is probably due to the presence of islands of PEDOT-rich grains interspersed within a network insulating PSS barriers.[56] Importantly, no such deviations in optoelectronic properties are observed for the FA-treated PEDOT:PSS films, indicating exceptional uniformity even for films with T = 99%. This is significant as such deviations always diminish the performance of transparent SCs at high T.[27] Networks formed from typical-sized discrete nano-objects, such as carbon nanotubes, graphene, or metallic wires, almost always show percolation effects as film thickness is reduced.[37]

The superlative optical and electrical properties of secondary-doped PEDOT:PSS films make this material ideal for the production of transparent SC electrodes. The low optical conductivity means that for a given transmittance (e.g., T = 95%) the electrode can be relatively thick. For a given intrinsic volumetric capacitance, this will result in a larger areal capacitance ($C_A = C_V t$). Additionally, high DC conductivity will facilitate transport of stored charge to the external circuit, even for electrodes with high T.

Electrochemical Properties of Small-Area Electrodes. The capacitive charge storage properties of small-area PEDOT:PSS films were characterized in a three-electrode cell by cyclic voltammetry (CV). This allows characterization of the properties of the electrode material itself rather than a complete SC device. We first carried out CV measurements for a T = 95% film over a wide potential window (−0.8 to 1.0 V vs Ag/AgCl), shown in Supporting Information, Figure S3. On the basis of this, we chose a narrower potential window for all subsequent electrochemical measurements in a region where the electrode behavior was ideally capacitive (+0.1 to 0.7 V vs Ag/AgCl). Although future studies aimed at maximizing energy storage could focus on maximizing the potential window (eq 1), here we do not focus on this aspect of SC electrode performance.

Shown in Figure 2A are CV scans for a PEDOT:PSS film (T = 95%, $\dot{V}$ = 100 mV/s) before and after exposure to formic acid. A series resistor and capacitor circuit provides a simple model for the electrode current response to a linear potential sweep, expressed as a function of time, t[57]

$$j = C_A \dot{V}(1 - e^{-t/\tau}) \quad (6)$$

Here, j is the current density, $\dot{V} = dV/dt$ is the scan rate, C_A is the rate-independent electrode areal capacitance already

DOI: 10.1021/acsami.5b03882
ACS Appl. Mater. Interfaces 2015, 7, 16495−16506

introduced, and $\tau = R_{ESR}C$ is the time constant. Here, R_{ESR} is the equivalent series resistance of the electrochemical circuit (here in a three-electrode configuration) and $C = C_A A$ is the capacitance of the electrode. The rapid current response of the FA-treated film compared with that of the as-prepared film indicates a dramatic reduction in τ. We believe this improved electrode response is overwhelmingly due to improved current collection through the plane of the film, as the treatment caused the R_s of this film to decrease by over 2 orders of magnitude, giving 205 ohm/sq, compared with 100 kohm/sq prior to the treatment. This view is also supported by the previous observation that the R_{ESR} of transparent SC electrodes scales linearly with R_s.[27] In addition, alternative explanations for the large reduction in τ are unlikely, such as being due to reduced electrode capacitance or other contributions to the R_{ESR} such as the electrolyte or electrode contact resistance.

To assess the electrochemical stability of the FA-treated films, 3500 repeated CV cycles were performed for both thin and thick samples (T = 67 and 95%) at a scan rate of 100 mV/s. By integrating the current passed per cycle, a capacitance retention ratio was calculated and plotted as a function of the number of CV cycles in Figure 2B. We observed a slight increase in capacitance within the first 1000 cycles (<3% for the thicker film and <1% for the thin film), probably due to minor rearrangement of the polymer film. With >99% retention for both films, the charge/discharge process is stable over this duration of cycling. The Figure 2B inset compares CV trace of the first and 3500th cycle for the T = 95% film, indicating some minor changes in features of the CV. Alongside the well-known stability of PEDOT,[41,58] these results suggest excellent cyclability of this material, a prerequisite for any promising SC electrode.

We then examined the charge storage properties of the small-area (1 × 1 cm^2) FA-treated PEDOT:PSS films in more detail. Here, CV measurements were obtained at a range of scan rates ($\dot{V}$ = 100−5000 mV/s), and the current density at midvoltage (0.4 V vs Ag/AgCl) was evaluated. In the ideal case, capacitive behavior is indicated by $j = C_A\dot{V}$.[59] We note that eq 6 reduces to this form when the electrode time constant is small relative to the discharge or recharging time (i.e., $\tau \ll \Delta V/\dot{V}$). Figure 2C shows such data obtained from CV measurements of films with different transmittance (T = 80−99%, t = 10−260 nm). The inset shows example CV traces for these films at 100 mV/s. Clearly, near ideal capacitive behavior predominates over a wide range of scan rates for all of these small-area films, even those at very high T. Similar behavior was observed for PEDOT:PSS-based SCs without an underlying current collector by Carlberg et al., which remain ideally capacitive at 200 mV/s.[41] For our films, only above ∼1000 mV/s do deviations become noticeable, corresponding to charge and discharge times less than ∼0.6 s. Closer inspection reveals that for thicker films (with lower R_s) the onset of this deviation shifts to greater scan rates. This provides a subtle indication that the transport limitations which determine R_{ESR} are likely due to the R_s contributions as opposed to ionic diffusion, for which we would expect the deviation onset to be independent of film transmittance.

Considering the data in Figure 2C, using the low scan rate range over which the electrode behavior is near ideally capacitive ($\dot{V}$ < 1000 mV/s), we extracted the rate-independent quantity, C_A, for each film from the intercept with the ordinate. This data has been plotted a function of film transmittance in Figure 2D. As expected, more transparent films store less charge for a given geometric area, simply because thinner films provide less capacitive material on the substrate surface. We measured C_A = 1.9 mF/cm^2 for a low transmittance film (T = 70%), decreasing to C_A = 0.18 mF/cm^2 for the most transparent film (T = 99%). To the best of our knowledge, the areal capacitance values of these FA-treated PEDOT:PSS films sets the state of the art for high-SC electrodes with high transmittance (T > 90%).

Provided that C_V is indeed constant for all film thicknesses, these data should be described by eq 3.[27] This equation describes the data well for all transmittances. Because this is equivalent to showing $C_A \propto t$ for all thicknesses,[27] this indicates that the electrolyte penetrates throughout the PEDOT:PSS films. Fitting gives C_V/σ_{op} = 1.7 F/S·cm^2, which can be considered to be a figure of merit for transparent capacitive electrodes (FoM$_c$). Alongside these PEDOT:PSS data, we have also included results from the transparent capacitor literature.[8,17,22,26,28−32,34] Note that this excludes reports where underlying ITO current collectors have been used.[18−25] We highlight that other than this work and that of King et al.,[27] to our knowledge, no other data has been presented for electrodes with T > 90%, the region of interest for transparent devices. Supporting Information, Figure S4, contains a reproduction of Figure 2D indicating the authors of the literature data, which were not included for clarity. Our PEDOT:PSS films have a much higher FoM$_c$ than that of the disordered SWNT films reported by King et al., which provide C_V/σ_{op} = 0.3 F/S·cm^2. In addition, while the capacitance of the SWNT network films deviate markedly from bulk-like behavior at T > 90% due to percolation effects,[27] the capacitance of these PEDOT:PSS films remain bulk-like even at very high transmittance (T = 99%). As discussed above, this is a key advantage of these sprayed PEDOT:PSS films compared to alternative transparent SC electrodes based on disordered nanomaterial network electrodes.

Equation 3 indicates that the capacitive performance of transparent SC electrodes depends strongly on C_V. However, this quantity is rarely calculated explicitly for transparent SC electrodes. We can determine the volumetric capacitance of this material using the fitted FoM$_c$ and the known σ_{op} of this material, yielding C_V = 41 F/cm^3. Despite the disparity between the FoM$_c$ of these PEDOT:PSS films (C_V/σ_{op} = 1.7 F/S·cm^2) and the SWNT films reported by King et al. (C_V/σ_{op} = 0.3 F/S·cm^2), it is interesting to note that these two materials have similar volumetric capacitances (C_V = 55 F/cm^3 for the SWNTs). Therefore, again, we can attribute the superior performance of PEDOT:PSS as a transparent SC charge storage film to its very low optical conductivity (σ_{op} = 24 S/cm compared with σ_{op} = 167 S/cm for the SWNTs). Using this value for the volumetric capacitance, we can calculate an approximate gravimetric capacitance of this materials using $C_M = C_V/\rho$. Here, we have measured density of a free-standing PEODT:PSS film as ρ = 1.2 g/cm^3, giving C_M = 34 F/g, a fairly typical value for an electrochemical double-layer capacitance. Although PEDOT is capable of pseudocapacitive charge storage through reduction at potenials ∼−0.2 V vs Ag/AgCl and subsequent reoxidization at ∼0.0 V (see Supporting Information, Figure S3), the use of such processes may not be suitable for transparent SC applications due to the associated electrochromism.[40]

Many electrode materials have been reported with substantially higher volumetric capacitance, particularly those making use of pseudocapacitive charge transfer reactions;

DOI: 10.1021/acsami.5b03882
ACS Appl. Mater. Interfaces 2015, 7, 16495−16506

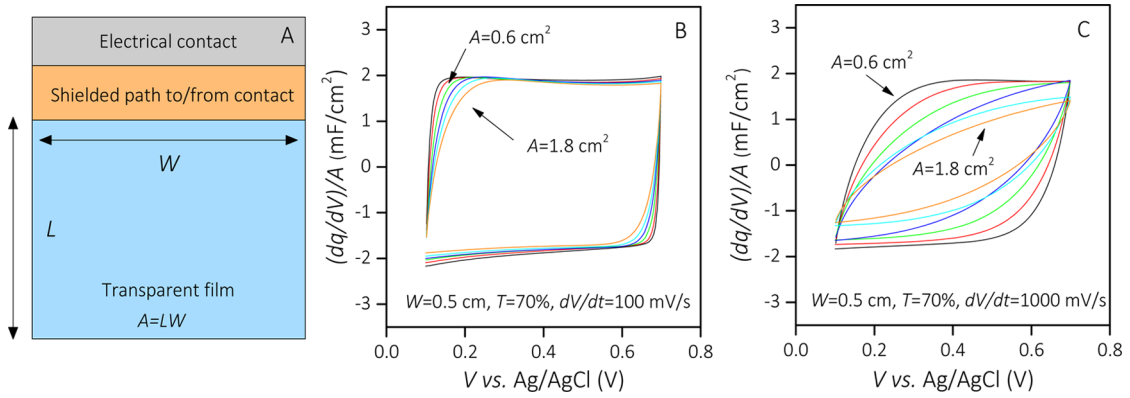

Figure 3. Effect of film lateral dimensions on CV behavior of FA-treated PEDOT:PSS films. (A) Diagram of electrode indicating length (L) and width (W) dimensions with relation to the electrical contact (top edge). CVs at (B) $\dot{V}$ = 100 mV/s and (C) $\dot{V}$ = 1000 mV/s for a T = 70% film. Film area is varied from A = 0.6 to 1.8 cm^2 by altering the length from L = 1.2 and 3.6 cm (width is constant, W = 0.5 cm). Current density is expressed as a differential capacitance.

Carlberg et al. reported 100 F/cm^3 for PEDOT:PSS films,[41] Ghaffari et al. measured 84 F/cm^3 for PEDOT:PSS-coated nanotubes, Largeot et al.[60] reported values ~100 F/cm^3 for nanotubes, and values as high as 1160 F/cm^3 have been achieved using MnO_2 composites.[61] The literature data in Figure 2D, which sits ahead of our PEDOT:PSS data in the low transmittance regime (Gao et al.[28] and Nam et al.[31]), suggests that higher FoM_c than that of these PEDOT:PSS films are possible (i.e., C_V/σ_{op} as high as 5 F/S·cm^2). These electrode materials could yield better capacitance at high transmittance values (T > 90%) if they could be produced thin enough while also avoiding percolation effects.[27] We suggest that this may be achieved by composite formation of secondary-doped PEDOT:PSS with another highly pseudocapacitive material such as manganese dioxide[62] to boost C_V without substantially increasing σ_{op}.

Considering Figure 2C, when the scan rate is large enough, the measured areal capacitance (which we will refer to as C/A and represents the accessible area capacitance) becomes less than the areal capacitance expected in the absence of electronic or ionic transport limitations (i.e., $C/A < C_A$). We can examine this scan rate dependence of the CV behavior more effectively by normalizing the measured current density to the scan rate, yielding a differential capacitance (i.e,. $j/\dot{V} = (dq/dV)/A$).[63] Figure 2E shows CV data expressed in this manner for a film with T = 99% at a variety of scan rates ($\dot{V}$ = 100−5000 mV/s). These demonstrate a reduction in accessible charge storage with scan rate due to the electrode time constant becoming comparable to the time available to accumulate or dispense charge. Although Figure 2C allowed extraction of the rate-independent areal capacitance, the measured areal capacitance, C/A, at a given scan rate is given by the total charge (q) passed divided by the voltage window (i.e., $C/A = (\Delta q/\Delta V)/A$). This value can be found at each scan rate by integrating CV data using

$$\frac{C}{A} = \frac{1}{(\Delta V)\dot{V}} \int_{v}^{v+\Delta V} j \, dV \tag{7}$$

Here, v is the starting voltage (0.1 V vs Ag/AgCl) and ΔV is the potential window (here, 0.6 V). The C/A is shown in Figure 2F for a number of films with different transmittance (T = 80−99%). The included dashed lines are the rate-independent C_A values obtained in Figure 2C. As expected, the C/A values approach C_A at low scan rates. The ratio of these quantities $((C/A)/C_A)$ provides a measure of the capacitance that is accessible at a given scan rate. For example, for the T = 99% film, 92% of C_A is accessible at 300 mV/s, whereas this decreases to 75% at 1000 mV/s. Although these deviations are not dramatic, it is important to note that these films are relatively small (1 × 1 cm^2). Given that real transparent SC devices are likely to use electrodes with larger dimensions than this, it is necessary to also characterize the charge storage behavior transparent films as a function of film size.

The Effect of Film Lateral Dimensions on CV Behavior. For a charge storage material with some value of C_V, when film thickness is constrained to provide some required transmittance (say, T = 90%), the only way to store more charge is by increasing the film volume via the lateral dimensions of the film. However, in the literature, the vast majority of transparent SC electrodes are tested with small active areas and obtained capacitance data is presented on either a per mass or per area basis. In general, no attempt is made to explore the scaling of absolute capacitance with electrode dimensions for larger area electrodes.

Here, we perform such a study, exploring the effect of both electrode length and width on the absolute capacitance. We define the electrode width, W, as the dimension parallel to the current collecting electrical contact at the upper film edge and electrode length, L, as the perpendicular dimension (see Figure 3A; note that we do not use a current collector between the PEDOT:PSS film and the PET support). Initially, we measured CVs for electrodes as a function of film L (and so area) while keeping the width constant (W = 0.5 cm). This was achieved by first characterizing the largest area film and then cutting off a small bottom section from the film to reduce L. For example, Figure 3B,C shows the area dependence of the CV response of these films at 100 and 1000 mV/s, respectively. Here, L was varied from 3.6 to 1.2 cm, resulting in a variation in film area from A = 1.8 to 0.6 cm^2. Again, the current density has been normalized to scan rate to enable its expression as a differential areal capacitance ($(dq/dV)/A$).

These results are interesting because they highlight the effect of both L and $\dot{V}$ on the measured areal capacitance. At the relatively slow scan rate of 100 mV/s, there is a small but noticeable increase in time constant as the sample length is increased, consistent with an increasing in-plane electrode resistance contributing to the R_{ESR} and a larger available capacitance, which together determine the electrode time

DOI: 10.1021/acsami.5b03882
ACS Appl. Mater. Interfaces 2015, 7, 16495−16506

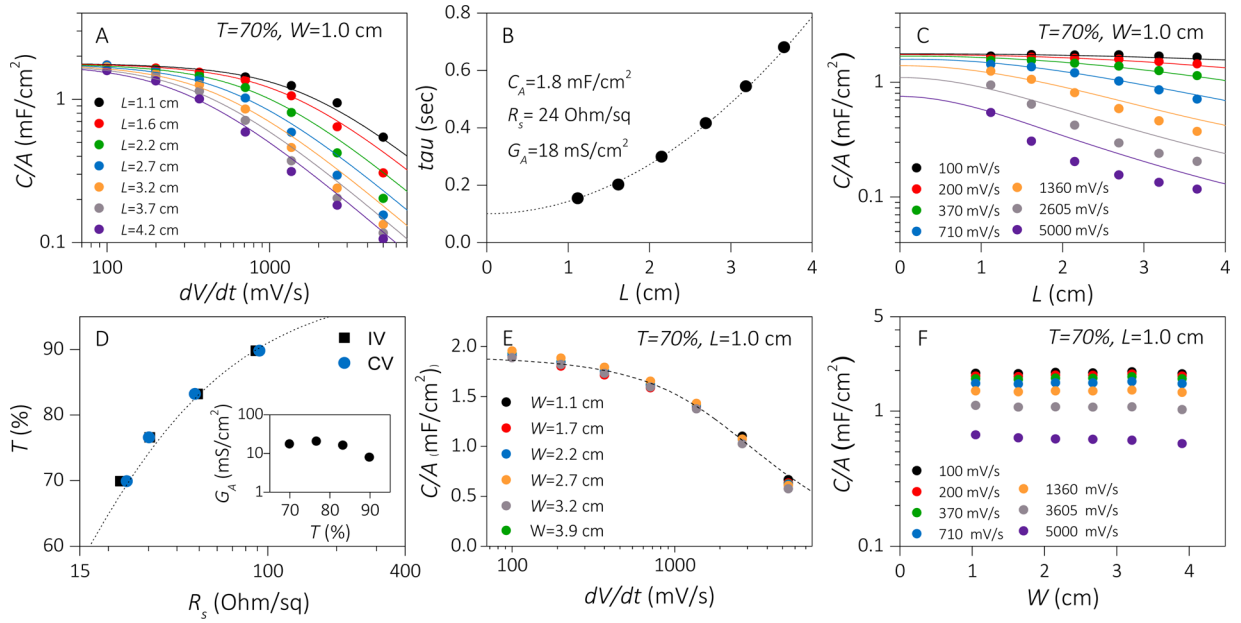

Figure 4. Size dependence of the charge storage properties of PEDOT:PSS films. (A) C/A data obtained by integrating the current passed for CVs at various $\dot{V}$ for a film with different sample lengths (L = 1.1−4.2 cm), keeping the width constant. Solid lines are fits of eq 9, providing the time constant, τ, as a function of sample length, plotted in (B). Here, the dashed line is a fit of eq 10, with C_A = 1.8 mF/cm^2, R_s = 24 ohm/sq, and G_A = 18 mS/cm^2 for this film. (C) C/A data plotted as a function of sample length for various $\dot{V}$. Using the parameters found in (B), eq 12 has been plotted with this data. (D) R_s values extracted from the L dependence analysis for various films and compared with those obtained by IV measurements. Inset shows electrolyte conductance values obtained for these films. (E) C/A obtained similarly as for (A), although here the film width is varied (W = 1.1−3.9 cm), keeping the length constant. (F) C/A plotted as a function of sample width at various $\dot{V}$.

constant. This will manifest itself as a slight reduction in C/A at a given $\dot{V}$. However, at the higher scan rate of 1000 mV/s, this effect is much more pronounced. As L is increased, significant increases in the time constant can be seen. These results imply that long electrodes will sustain reduced C/A compared to that expected for short ones, especially at high scan rates. This illustrates that the absolute capacitance of a potential device cannot simply be projected from the areal capacitance values measured for small-area samples.

We can quantify this behavior by calculating C/A from the CV scans by integration (eq 7). This has been performed for samples with a range of L (with W = 1.0 cm) with each one analyzed over a range of $\dot{V}$, shown in Figure 4A. It is clear from this data that the capacitance falls dramatically as both L and $\dot{V}$ are increased, as suggested above. These effects can be significant; at $\dot{V}$ = 1000 mV/s, and when L = 3.6 cm, C/A is a factor of 3 less than expected from the L = 1.2 cm sample, leading to no increase in absolute capacitance as the electrode area is increased.

The decrease in C/A with increasing L can be understood as follows. As the electrode gets longer, the average resistance felt by electrons moving from the electrode contact through the film increases. This, in turn, increases the time constant ($\tau = R_{ESR}C$), causing a slower current rise on voltage reversal. Because the capacitance is calculated by integration of the CV curve, this results in lower measured areal capacitances than those expected in the absence of charge transport limitations (equivalent to $C/A < C_A$). We can model this quantitatively by combining eqs 6 and 7 to give

$$\frac{C}{A} = \frac{1}{\Delta V}\int_{v}^{v+\Delta V} [C_A(1 - e^{-t/\tau})]dV \qquad (8)$$

All of the terms appearing have been described earlier. Changing the variable from V to t ($dV = \dot{V}\,dt$) and integrating gives

$$\frac{C}{A} = C_A\left[1 - \frac{\dot{V}\tau}{\Delta V}(1 - e^{-\Delta V/\dot{V}\tau})\right] \qquad (9)$$

This describes the dependence of the measured areal capacitance, C/A, on the rate-independent areal capacitance, C_A, the scan rate, $\dot{V}$, and the time constant, τ.

We can use eq 9 to fit the C/A vs $\dot{V}$ data shown in Figure 4A, finding very good agreement for all samples lengths. From the fits, we find that, for this particular thickness of PEDOT:PSS (T = 70%, t = 432 nm), the rate-independent areal capacitance is C_A = 1.9 mF/cm^2. Note that we expect a value of 1.8 mF/cm^2 for a film with this transmittance based on the FoM$_c$ (Figure 2D). It is worth noting that by expanding the exponential in eq 9 it can be shown that, at high scan rates, $C/A \propto \dot{V}^{-1}$ in the situation where the capacitance is limited by the electrical properties of the electrode. This is in comparison to the more well-known scenario where the measured area capacitance at high rates is limited by ionic diffusion and $C/A \propto \dot{V}^{-1/2}$.[57] This allows the potential for rapid assessment of the limiting factor from the capacitance versus scan rate data.

In addition, we find that the time constant (from the fit) varies considerably with sample length, as shown in Figure 4B. We can understand this by noting that the time constant is given by $\tau = R_{ESR}C$, where C reflects the available capacitance of the electrode and R_{ESR} reflects the series combination of electrode and electrolyte resistances associated with this electrode ($R_{ESR} = R_{electrode} + R_{electrolyte}$). Here, we assume that all of the resistances associated with electrical contacts and the external leads are small enough to be ignored. We can express these three parameters in terms of the electrode geometry: the

DOI: 10.1021/acsami.5b03882
ACS Appl. Mater. Interfaces 2015, 7, 16495−16506

capacitance as ($C = C_A LW$), the electrolyte resistance as the inverse of the electrolyte conductance per unit area, G_A, multiplied by area, $1/G_A LW$, and the electrode resistance as the sheet resistance multiplied by electrode aspect ratio, $R_s L/W$. When combined, these given an expression for the time constant that is a function of electrode length, L, as shown in eq 10.

$$\begin{aligned}\tau &= C(R_{\text{electrode}} + R_{\text{electrolyte}}) \\ &= C_A LW\left(R_s\frac{L}{W} + \frac{1}{G_A LW}\right) \\ &= C_A R_s L^2 + \frac{C_A}{G_A}\end{aligned} \tag{10}$$

As shown in Figure 4B, eq 10 fits the experimental data extremely well, allowing extraction values of R_s = 24 ohm/sq and G_A= 18 mS/cm^2 for this sample. This film had a sheet resistance of 25 ohm/sq when measured by current−voltage curves. This length dependence analysis has been repeated for a number of films with differing transmittance values (T = 70−90%, shown in Supporting Information, Figure S5). The extracted R_s values have been plotted alongside the R_s data obtained by current−voltage measurements in Figure 4D, showing excellent agreement. Shown in the inset of this figure are the G_A values that were obtained. Although the true electrolyte conductance should be invariant of film thickness, the values obtained here differ slightly due to the fact that this parameter includes other resistance terms ignored for this analysis, in particular, the through film resistance between the electrode and electrical contact (shown in orange in Figure 3A). Given that $G_A = l\sigma_{\text{electrolyte}}$, where $\sigma_{\text{electrolyte}}$ is the electrolyte conductivity and l is the electrode separation (here, ∼1 cm), this suggests that $\sigma_{\text{electrolyte}} \sim 15$ mS/cm, which is within a factor of 5 of the expected value for a 0.5 M K_2SO_4 solution (75 mS/cm at 20 °C).[64]

As the areal capacitance and sheet resistance are related to the film thickness via $C_A = C_V t$ and $R_s = (\sigma_{DC} t)^{-1}$, it is possible to write eq 10 in an alternative form

$$\tau = \frac{C_V}{\sigma_{DC}}L^2 + \frac{C_V}{G_A}t \tag{11}$$

This form is of interest because it depends on intrinsic and dimensional parameters only and includes the dependence on electrode thickness.

We can also apply this model to the data for C/A as a function of L. To do this, we combine eqs 9 and 10 to give

$$\begin{aligned}\frac{C}{A} = C_A\Bigg[1 - \frac{\dot{V}}{\Delta V}\left(C_A R_s L^2 + \frac{C_A}{G_A}\right) \\ \times\left(1 - \exp\left[\frac{-\Delta V/\dot{V}}{(C_A R_s L^2 + C_A/G_A)}\right]\right)\Bigg]\end{aligned} \tag{12}$$

As all parameters in this expression are known (C_A, R_s, G_A, ΔV), we can plot eq 12 as a function of L for different $\dot{V}$ and compare with the experimental data presented in Figure 3C. Although we find good agreement at low rates, the fit is noticeably poorer for $\dot{V}$ > 1000 mV/s. This is not unexpected; at such high charge/discharge rates, a series resistor−capacitor combination is no longer an appropriate representation of this electrode system. To provide evidence for this, we have performed a separate electrochemical impedance spectroscopy analysis of the behavior of these electrode as a function of sample L, which has been included in the Supporting Information. This analysis demonstrates that under rapid charge−discharge conditions (in this case, a high-frequency voltage perturbation) a Warburg-like electrode response is observed, indicating that the electrode's behavior becomes limited by electrical transport to the back of the film (Supporting Information, Figure S6). As such, a more sophisticated model for this electrode system consists of a single-arm transmission line with a distributed capacitance that may be accessed via an incremental resistance through the plane of the film (Supporting Information, Figure S7). However, we feel that the series resistor−capacitor circuit model that has been applied to CV electrode behavior provides a simple and insightful treatment of lateral dimension effects that is applicable over a wide range of charge−discharge rates relevant for SC operation.

In addition to the sample length dependence of capacitive charge storage, for completeness, we have also performed the same CV analysis for the converse situation; with the sample length kept constant (L = 0.5 cm) while varying the width (W = 0.8−4.5 cm). As shown in Figure 4E,F, the W dependence is straightforward. Although C/A falls with scan rate in line with eq 9, it is invariant with sample width, W, at all rates. This is as expected because the sample width does not appear in eq 12.

This simple CV analysis demonstrates the influence of film lateral dimensions on the charging and discharging time constant, which, in turn, causes C/A to be diminished for longer films. Although it is fairly intuitive, this behavior has not been identified or studied in detail previously, and we feel these insights will be very important for future transparent SC design.

Limitations of Sample Length and Scan Rate. As indicated by Figure 4A,C, C/A begins to fall once either the scan rate or sample length are increase above a certain value. The design of real large-area supercapacitor electrodes would be facilitated by an understanding of the relationship between sample length and scan rate when the effective capacitance begins to deviate from the rate-independent value. The model above can be used to provide this relationship.

The C/A as obtained from eq 9 is essentially constant for a low values of $\dot{V}\tau/\Delta V$. By analysis of eq 9 (i.e., by expanding the exponential and equating the zeroth-order, low-rate approximation with the second-order, high-rate approximation), it can be shown that the C/A begins to fall off approximately when $\dot{V}\tau/\Delta V$ = 0.5. Using eq 11, this means that for a given sample length the maximum scan rate before the C/A begins to fall-off is given by

$$\dot{V}_{\max} = \frac{\Delta V/2}{(C_V L^2/\sigma_{DC} + C_V t/G_A)} \tag{13}$$

or, alternatively, the maximum sample length for effective performance at a given scan rate

$$L_{\max} = \sqrt{\frac{\sigma_{DC}}{C_V}\left(\frac{\Delta V/2}{\dot{V}} - \frac{C_V t}{G_A}\right)} \tag{14}$$

We note that these expressions can be expressed alternatively as a function of transmittance rather than thickness using eq 5. However, for the sake of simplicity, we leave them in the current form.

These expressions show that as the electrode length is increased the maximum rate at which energy can be extracted,

DOI: 10.1021/acsami.5b03882
ACS Appl. Mater. Interfaces 2015, 7, 16495−16506

as expressed by $\dot{V}_{max}$, falls rapidly. Attempts to extract charge at a higher rate will result in a fall-off in effective capacitance (and so accessible energy). To demonstrate, in Figure 5, we use eq 13 to plot the maximum achievable scan rate as a function of L using the parameters established above for PEDOT:PSS and the electrolyte used here: σ_{DC} = 936 S/cm, C_V = 41 F/cm^3, ΔV = 0.6 V, and G_A = 18 mS/cm^2. This graph clearly demonstrates the limitations on the performance transparent SC electrodes in terms of size or charge and discharge rate. For example, if the electrode transparency is set at 90% (effectively setting the thickness) and a maximum scan rate of 1 V/s is required, then the sample length can be no more than 1 cm before the C/A starts falling from its rate-independent value.

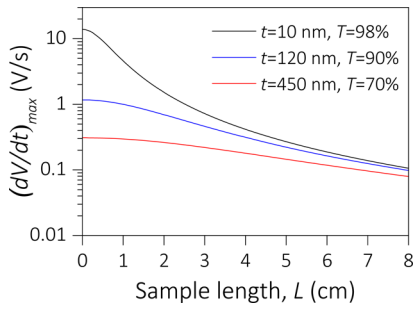

Figure 5. Scan rate above which the CV response deviates from the C_A as a function of sample length, L. The three traces show the dependence on film transmittance (and thickness) for three different films.

Large-Area Device Measurements. Presently, the largest transparent SC device described in the literature[26] is only 4.5 cm^2. Given that applications will no doubt require larger area devices, capable of greater absolute charge storage, it is necessary to demonstrate what kind of performance is possible. The spray system used in this work is capable of producing films with dimensions of 18 × 18 cm^2, potentially giving a device area of 324 cm^2. However, as shown in the previous section, the absolute capacitance of devices with an L dimension greater than ∼5 cm are not able to store significantly more charge at the charge/discharge rates of interest for SC applications (∼100s of mV/s). Accordingly, here, we present measurements for devices with dimensions of W = 18 cm and L ≤ 6 cm), giving a maximum electrode footprint of 108 cm^2. A pair of films produced from a single 18 cm × 18 cm piece is shown in Figure 6A with film transmittance of 95%. These electrodes are substantially larger than those used in any transparent SC device published previously.

Using a two-electrode configuration, these electrodes were tested in a large beaker by cyclic voltammetry at a variety of scan rates (50−1500 mV/s). Shown in Figure 6B are CVs expressed as differential capacitance ($(dq/dV)/A$) for four device footprints (A = 18−108 cm^2) at 50 mV/s. Measured areal capacitances were found by integrating the current passed over the potential window and are plotted vs device length for a range of scan rates in Figure 6C. In all cases, C/A falls with sample length, although this phenomenon is less severe for a low scan rates, as was observed from single-electrode measurements. Shown in Figure 6D is the absolute capacitance (i.e., $C = LW \times (C/A)$) plotted vs electrode length. For the largest area device, we measured 12.5 mF at 50 mV/s. It is clear from this data that the absolute capacitance increases at best sublinearly with length over the size range. This is entirely consistent with the results of Figure 5 and shows that, for combinations of long lengths and high rates, increasing the electrode length gives fast diminishing returns. We show this more clearly in Figure 6E by plotting the absolute capacitance as a function of rate for two electrode lengths, L = 1 and 6 cm. It is clear from this graph that while at low rates a 6-fold increase in electrode length results in a doubling of capacitance,

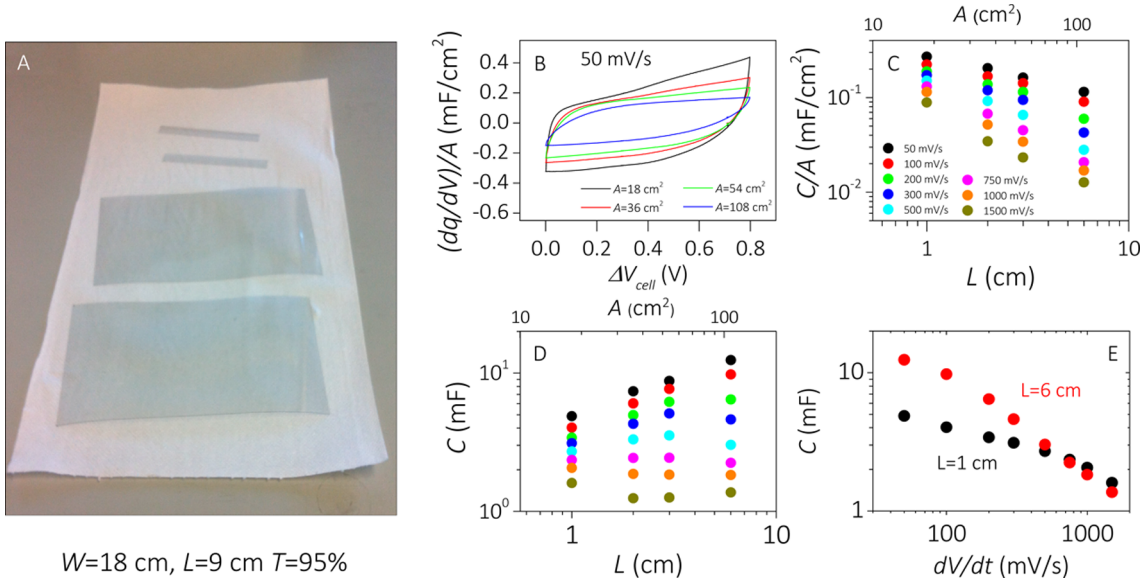

Figure 6. Two-electrode charge storage measurements for various transparent SCs (T_{single} = 95%). Electrode width was kept constant (W = 18 cm) and length was varied (L = 1−6 cm) to produce device areas from A = 18 to 108 cm^2. (A) Photo of two large-area sprayed PEDOT:PSS films (18 × 9 cm^2). (B) CVs obtained at 50 mV/s for the different device areas, expressed as a differential capacitance. (C) C/A as a function of device length, found by integration of CVs at various scan rates (dV/dt = 50−1500 mV/s). (D) Absolute capacitance as a function of device length at various scan rates. The max capacitance for the largest device was 12.5 mF (dV/dt = 50 mV/s). (E) Absolute capacitance as a function of scan rate for L = 1 and 6 cm (corresponding to A = 18 and 108 cm^2).

DOI: 10.1021/acsami.5b03882
ACS Appl. Mater. Interfaces 2015, 7, 16495−16506

at high rates, no benefit is seen from the electrode length increase.

As shown above, our largest area device gave C = 12.5 mF at 50 mV/s for a total transmittance of 90% (considering light absorption only by the electrode materials). In comparison, Jung et al. reported a transparent SC device with A = 4.5 cm^2 composed of electrodes with T = 71% at 500 nm, which gave a capacitance of 2.1 mF by constant current charge−discharge measurements (j = 5 $\mu A/cm^2$).[26] Although this value is 5 times less than reported here, care must be taken when making comparison. This is because the two devices possess different aspect ratio and different transmittance and were characterized by different electrochemical techniques.

CONCLUSIONS

This work furthers our understanding of the properties of transparent SC electrodes by characterizing PEDOT:PSS ultrathin electrodes in terms of three key materials properties: the optical conductivity, σ_{op}, the DC electrical conductivity, σ_{DC}, and the volumetric capacitance, C_V. Together, these determine the performance of a given transparent supercapacitor material, which may be summarized as an electrical and capacitive figure of merit for transparent supercapacitors; $FoM_e = \sigma_{DC}/\sigma_{op}$ and $FoM_c = C_V/\sigma_{op}$. Use of these metrics will facilitate rigorous comparison of candidate material systems for application as transparent SC electrodes, necessary for continued development of this field. The use of a spray coating deposition system combined with a secondary doping treatment using formic acid enabled the production high-quality PEDOT:PSS films without percolation effects even for very high transmittance (T = 99%).

This work also identifies lateral dimension effects that cause the measured areal capacitance to be lower than expected when scaling up the electrode area (i.e., A > 1 cm^2). These effects occur due to the need for current collection through the plane of the film and have implications for the capacitance that is available when using electrodes with a given lateral size when charged/discharged at a given rate. Accordingly, to assist with transparent supercapacitor design, we have developed simple equations that take these effects into account, enabling the analysis of data for capacitance versus rate or electrode dimensions. This behavior will predominate situations where the thin film material acts as the charge storage material and current collector simultaneously and, as such, is highly relevant for printed electronics applications.

METHODS

Film Preparation. An aqueous dispersion of PEDOT:PSS was obtained from Heraeus (Clevios PH 1000) and diluted with water to a concentration of 0.75 mg/mL. This was then used to produce PEDOT:PSS films on poly(ethlyene terephthalate) (PET) substrates using the method described in McCarthy et al.[53] In brief, the diluted polymer solution was loaded into a graduated reservoir and attached to a Harddner and Steenbeck Infinity airbrush spray system. Control over the airbrush was provided by a Janome JR2300N robot. The PET substrates were cleaned with surfactant solution and isopropanol prior to use and placed on the robot substrate stage, heated to 110 °C. Further details regarding the spraying parameters employed can be found in the Supporting Information.

The film lateral dimensions were controlled by the spraying program, limited by the dimensions of the substrate state (here, 18 cm × 18 cm). The thickness of the films was controlled by the number of repeated passes made by the spray, which delivers a greater total volume of polymer solution onto a given area of the substrate. Films were subsequently characterized as-prepared or subject to a formic acid (FA) post-treatment. This involved submerging the PEDOT:PSS films into the FA for 5 s and then allowing the films to dry in air.

Optoelectrical Characterization of Films. Optical transmittance spectra of the PEDOT:PSS films were obtained in the visible range (400−800 nm) using a Cary 600i spectrophotometer. In all cases, the PET background absorbance was subtracted. Film thickness was determined by contact profilometry (Dektak 6M, Veeco Instruments) for PEDOT:PSS films sprayed separately onto glass substrates. Here, film thickness values were taken as the mean thickness obtained by four height profiles obtained for different regions of the film. These measurements were performed after exposure to FA, as such secondary doping treatments are known to alter the film density.[53] The four-point probe technique was used to characterize the DC electrical properties of the films. To do so, electrodes contacts were created on the film surface using an alcohol-based conductive silver paint (Agar Scientific). The electrode separation and width were ∼1 and ∼0.5 cm, respectively. Current−voltage curves were obtained using a Keithley 2400 source meter.

Electrochemical Characterization of Films. Electrochemical testing was carried out in a three-electrode cell consisting of a carbon counter electrode and Ag/AgCl reference. The electrolyte used was 0.5 M K_2SO_4(aq). PEDOT:PSS working electrodes were formed by cutting strips from the main film and confining the electrolyte exposed area using adhesive tape. Silver paint was again used to form contacts to the external circuit. The electrolyte-exposed area was varied during different experiments. Here, we have defined the electrode width (W) to be the dimension parallel to the electrolyte solution and the length (L), the perpendicular dimension (i.e., greater values of L are more distant from the contact). The specific dimensions used for various measurements are indicated in the Results and Discussion. For the L and W dependence measurements, a large electrode was prepared, which was sequentially cut to the required smaller dimensions after the necessary measurements for a given size were completed.

Electrochemical testing using the three-electrode cell consisted of cyclic voltammetry and electrochemical impedance spectroscopy. CVs were obtained between the potential limits of 0.1 and 0.7 V vs the Ag/AgCl reference couple. Scan rates were varied from 100 to 5000 mV/s. Potentiostatic EIS was carried out at a DC bias of 0.4 V vs Ag/AgCl using a 10 mV AC perturbation varying between 0.1 Hz and 100 kHz. Immediately prior to acquiring the EIS spectra, working electrodes were conditioned at the as-mentioned DC bias for 3 min. This DC bias was chosen as the midpotential used for the CV measurements. To determine a value for the density of FA-treated PEDOT:PSS, a free-standing film was prepared by evaporative casting into a Teflon mold and measuring both its mass and dimensions.

Symmetric two-electrode measurements were performed in a large beaker containing 0.5 M K_2SO_4(aq) electrolyte. For these measurements, two films of equal dimensions and transmittance were positioned 1 mm apart. Here, CVs were performed using films with different areas. This was achieved by varying the film length ($L \leq 6$ cm) while holding the width constant (W = 18 cm), giving a maximum film area of 108 cm^2.

ASSOCIATED CONTENT

Supporting Information

(1) Details of the airbrush system's parameters, (2) data regarding the effect of FA treatment on the PEDOT:PSS transmittance spectra and absence of percolation effects for ultrathin films, (3) method preparation of Iljin SWNT dispersions, (4) a reproduction of Figure 2D to indicate the authors of the included literature data, and (5) an electrochemical impedance spectroscopy analysis of the L dependence of the electrode's AC behavior. The Supporting Information is available free of charge on the ACS Publications website at DOI: 10.1021/acsami.5b03882.

DOI: 10.1021/acsami.5b03882
ACS Appl. Mater. Interfaces 2015, 7, 16495−16506

AUTHOR INFORMATION

Corresponding Author

*E-mail: colemaj@tcd.ie.

Notes

The authors declare no competing financial interest.

ACKNOWLEDGMENTS

The authors would like to thank Dr. Joseph McCarthy and Richard Coull for discussions and assistance with use of the robotic spraying system. We have received support from the Science Foundation Ireland (SFI) funded centre AMBER (SFI/12/RC/2278). In addition, J.N.C. acknowledges the European Research Council (SEMANTICS) and SFI (11/PI/1087) for financial support.

REFERENCES

(1) Sirringhaus, H.; Kawase, T.; Friend, R. H.; Shimoda, T.; Inbasekaran, M.; Wu, W.; Woo, E. P. High-Resolution Inkjet Printing of All-Polymer Transistor Circuits. *Science* **2000**, *290* (5499), 2123−2126.

(2) Park, J.-U.; Hardy, M.; Kang, S. J.; Barton, K.; Adair, K.; Mukhopadhyay, D. k.; Lee, C. Y.; Strano, M. S.; Alleyne, A. G.; Georgiadis, J. G.; et al. High-resolution electrohydrodynamic jet printing. *Nat. Mater.* **2007**, *6* (10), 782−789.

(3) Torrisi, F.; Hasan, T.; Wu, W.; Sun, Z.; Lombardo, A.; Kulmala, T. S.; Hsieh, G.-W.; Jung, S.; Bonaccorso, F.; Paul, P. J.; et al. Inkjet-Printed Graphene Electronics. *ACS Nano* **2012**, *6* (4), 2992−3006.

(4) Ishikawa, F. N.; Chang, H.-k.; Ryu, K.; Chen, P.-c.; Badmaev, A.; Gomez De Arco, L.; Shen, G.; Zhou, C. Transparent Electronics Based on Transfer Printed Aligned Carbon Nanotubes on Rigid and Flexible Substrates. *ACS Nano* **2009**, *3* (1), 73−79.

(5) Lee, S.-K.; Kim, B. J.; Jang, H.; Yoon, S. C.; Lee, C.; Hong, B. H.; Rogers, J. A.; Cho, J. H.; Ahn, J.-H. Stretchable Graphene Transistors with Printed Dielectrics and Gate Electrodes. *Nano Lett.* **2011**, *11* (11), 4642−4646.

(6) Lee, S.; Lee, K.; Liu, C.-H.; Kulkarni, G. S.; Zhong, Z. Flexible and transparent all-graphene circuits for quaternary digital modulations. *Nat. Commun.* **2012**, *3*, 1018.

(7) Wu, Z.; Chen, Z.; Du, X.; Logan, J. M.; Sippel, J.; Nikolou, M.; Kamaras, K.; Reynolds, J. R.; Tanner, D. B.; Hebard, A. F.; et al. Transparent, Conductive Carbon Nanotube Films. *Science* **2004**, *305* (5688), 1273−1276.

(8) Sorel, S.; Khan, U.; Coleman, J. N. Flexible, transparent dielectric capacitors with nanostructured electrodes. *Appl. Phys. Lett.* **2012**, *101* (10), 103106−103106−5.

(9) Kudo, A.; Yanagi, H.; Ueda, K.; Hosono, H.; Kawazoe, H.; Yano, Y. Fabrication of transparent p−n heterojunction thin film diodes based entirely on oxide semiconductors. *Appl. Phys. Lett.* **1999**, *75* (18), 2851−2853.

(10) Ju, S.; Facchetti, A.; Xuan, Y.; Liu, J.; Ishikawa, F.; Ye, P.; Zhou, C.; Marks, T. J.; Janes, D. B. Fabrication of fully transparent nanowire transistors for transparent and flexible electronics. *Nat. Nanotechnol.* **2007**, *2* (6), 378−384.

(11) Xiao, L.; Chen, Z.; Feng, C.; Liu, L.; Bai, Z.-Q.; Wang, Y.; Qian, L.; Zhang, Y.; Li, Q.; Jiang, K.; et al. Flexible, Stretchable, Transparent Carbon Nanotube Thin Film Loudspeakers. *Nano Lett.* **2008**, *8* (12), 4539−4545.

(12) Nakamura, H.; Tohyama, K.; Tanaka, M.; Shinohara, S.; Tokunaga, Y.; Kurusu, F.; Koide, S.; Gotoh, M.; Karube, I. Development of a package-free transparent disposable biosensor chip for simultaneous measurements of blood constituents and investigation of its storage stability. *Biosens. Bioelectron.* **2007**, *23* (5), 621−626.

(13) Fan, F.-R.; Lin, L.; Zhu, G.; Wu, W.; Zhang, R.; Wang, Z. L. Transparent Triboelectric Nanogenerators and Self-Powered Pressure Sensors Based on Micropatterned Plastic Films. *Nano Lett.* **2012**, *12* (6), 3109−3114.

(14) Lunt, R. R.; Bulovic, V. Transparent, near-infrared organic photovoltaic solar cells for window and energy-scavenging applications. *Appl. Phys. Lett.* **2011**, *98* (11), 113305.

(15) Choi, D.; Choi, M.-Y.; Choi, W. M.; Shin, H.-J.; Park, H.-K.; Seo, J.-S.; Park, J.; Yoon, S.-M.; Chae, S. J.; Lee, Y. H.; et al. Fully Rollable Transparent Nanogenerators Based on Graphene Electrodes. *Adv. Mater.* **2010**, *22* (19), 2187−2192.

(16) Yang, Y.; Jeong, S.; Hu, L.; Wu, H.; Lee, S. W.; Cui, Y. Transparent lithium-ion batteries. *Proc. Natl. Acad. Sci. U. S. A.* **2011**, *108*, 13013−13018.

(17) Chen, P.-C.; Shen, G.; Sukcharoenchoke, S.; Zhou, C. Flexible and transparent supercapacitor based on In2O3 nanowire/carbon nanotube heterogeneous films. *Appl. Phys. Lett.* **2009**, *94* (4), 043113.

(18) Invernale, M. A.; Seshadri, V.; Mamangun, D. M. D.; Ding, Y.; Filloramo, J.; Sotzing, G. A. Polythieno[3,4-b]thiophene as an Optically Transparent Ion-Storage Layer. *Chem. Mater.* **2009**, *21* (14), 3332−3336.

(19) Sugimoto, W.; Yokoshima, K.; Ohuchi, K.; Murakami, Y.; Takasu, Y. Fabrication of Thin-film, Flexible, and Transparent Electrodes Composed of Ruthenic Acid Nanosheets by Electrophoretic Deposition and Application to Electrochemical Capacitors. *J. Electrochem. Soc.* **2006**, *153*, A255−A260.

(20) Moser, F.; Athouel, L.; Crosnier, O.; Favier, F.; Belanger, D.; Brousse, T. Transparent electrochemical capacitor based on electrodeposited MnO2 thin film electrodes and gel-type electrolyte. *Electrochem. Commun.* **2009**, *11* (6), 1259−1261.

(21) Yu, A.; Roes, I.; Davies, A.; Chen, Z. Ultrathin, transparent, and flexible graphene films for supercapacitor application. *Appl. Phys. Lett.* **2010**, *96*, 253105.

(22) Ge, J.; Cheng, G.; Chen, L. Transparent and flexible electrodes and supercapacitors using polyaniline/single-walled carbon nanotube composite thin films. *Nanoscale* **2011**, *3* (8), 3084−3088.

(23) Hu, Y.; Zhu, H.; Wang, J.; Chen, Z. Synthesis of layered birnessite-type manganese oxide thin films on plastic substrates by chemical bath deposition for flexible transparent supercapacitors. *J. Alloys Compd.* **2011**, *509* (42), 10234−10240.

(24) Nakayama, M.; Okamura, K.; Athouël, L.; Crosnier, O.; Brousse, T. Fabrication of a Transparent Supercapacitor Electrode Consisting of Mn-Mo Oxide/CNT Nanocomposite. *ECS Trans.* **2012**, *41* (22), 53−64.

(25) Ryu, I.; Yang, M.; Kwon, H.; Park, H. K.; Do, Y. R.; Lee, S. B.; Yim, S. Coaxial RuO2−ITO Nanopillars for Transparent Supercapacitor Application. *Langmuir* **2014**, *30* (6), 1704−1709.

(26) Jung, H. Y.; Karimi, M. B.; Hahm, M. G.; Ajayan, P. M.; Jung, Y. J. Transparent, flexible supercapacitors from nano-engineered carbon films. *Sci. Rep.* **2012**, *2*, 773.

(27) King, P. J.; Higgins, T. M.; De, S.; Nicoloso, N.; Coleman, J. N. Percolation Effects in Supercapacitors with Thin, Transparent Carbon Nanotube Electrodes. *ACS Nano* **2012**, *6*, 1732.

(28) Gao, K.; Shao, Z.; Wu, X.; Wang, X.; Zhang, Y.; Wang, W.; Wang, F. Paper-based transparent flexible thin film supercapacitors. *Nanoscale* **2013**, *5* (12), 5307.

(29) Gao, Y.; Zhou, Y. S.; Xiong, W.; Jiang, L. J.; Mahjouri-samani, M.; Thirugnanam, P.; Huang, X.; Wang, M. M.; Jiang, L.; Lu, Y. F. Transparent, flexible, and solid-state supercapacitors based on graphene electrodes. *APL Mater.* **2013**, *1* (1), 012101.

(30) Lin, H.; Li, L.; Ren, J.; Cai, Z.; Qiu, L.; Yang, Z.; Peng, H. Conducting polymer composite film incorporated with aligned carbon nanotubes for transparent, flexible and efficient supercapacitor. *Sci. Rep.* **2013**, *3*, 1353.

(31) Nam, I.; Park, S.; Kim, G.-P.; Park, J.; Yi, J. Transparent and ultra-bendable all-solid-state supercapacitors without percolation problems. *Chem. Sci.* **2013**, *4* (4), 1663−1667.

(32) Niu, Z.; Zhou, W.; Chen, J.; Feng, G.; Li, H.; Hu, Y.; Ma, W.; Dong, H.; Li, J.; Xie, S. A Repeated Halving Approach to Fabricate Ultrathin Single-Walled Carbon Nanotube Films for Transparent Supercapacitors. *Small* **2013**, *9* (4), 518−524.

DOI: 10.1021/acsami.5b03882
ACS Appl. Mater. Interfaces 2015, 7, 16495−16506

(33) Chen, T.; Peng, H.; Durstock, M.; Dai, L. High-performance transparent and stretchable all-solid supercapacitors based on highly aligned carbon nanotube sheets. *Sci. Rep.* **2014**, *4*, 3612.
(34) Chen, T.; Xue, Y.; Roy, A. K.; Dai, L. Transparent and Stretchable High-Performance Supercapacitors Based on Wrinkled Graphene Electrodes. *ACS Nano* **2014**, *8* (1), 1039−1046.
(35) Fan, X.; Chen, T.; Dai, L. Graphene networks for high-performance flexible and transparent supercapacitors. *RSC Adv.* **2014**, *4* (70), 36996−37002.
(36) Kim, Y. H.; Sachse, C.; Machala, M. L.; May, C.; Müller-Meskamp, L.; Leo, K. Highly Conductive PEDOT:PSS Electrode with Optimized Solvent and Thermal Post-Treatment for ITO-Free Organic Solar Cells. *Adv. Funct. Mater.* **2011**, *21* (6), 1076−1081.
(37) De, S.; Coleman, J. N. The effects of percolation in nanostructured transparent conductors. *MRS Bull.* **2011**, *36* (10), 774−781.
(38) Ahlswede, E.; Mühleisen, W.; bin Moh Wahi, M. W.; Hanisch, J.; Powalla, M. Highly efficient organic solar cells with printable low-cost transparent contacts. *Appl. Phys. Lett.* **2008**, *92* (14), 143307.
(39) Tait, J. G.; Worfolk, B. J.; Maloney, S. A.; Hauger, T. C.; Elias, A. L.; Buriak, J. M.; Harris, K. D. Spray coated high-conductivity PEDOT:PSS transparent electrodes for stretchable and mechanically-robust organic solar cells. *Sol. Energy Mater. Sol. Cells* **2013**, *110* (0), 98−106.
(40) Elschner, A.; Kirchmeyer, S.; Lovenich, W.; Merker, U.; Reuter, K. *PEDOT: Principles and Applications of an Intrinsically Conductive Polymer*, 1st ed.; CRC Press: Boca Raton, FL, 2010; p 377.
(41) Carlberg, J. C.; Inganäs, O. Poly(3,4-ethylenedioxythiophene) as Electrode Material in Electrochemical Capacitors. *J. Electrochem. Soc.* **1997**, *144* (4), L61−L64.
(42) Dressel, M.; Grüner, G. *Electrodynamics of Solids: Optical Properties of Electrons in Matter*; Cambridge University Press: Cambridge, 2002; p 490.
(43) Martin, B. D.; Nikolov, N.; Pollack, S. K.; Saprigin, A.; Shashidhar, R.; Zhang, F.; Heiney, P. A. Hydroxylated secondary dopants for surface resistance enhancement in transparent poly(3,4-ethylenedioxythiophene)−poly(styrenesulfonate) thin films. *Synth. Met.* **2004**, *142* (1−3), 187−193.
(44) De, S.; Higgins, T. M.; Lyons, P. E.; Doherty, E. M.; Nirmalraj, P. N.; Blau, W. J.; Boland, J. J.; Coleman, J. N. Silver Nanowire Networks as Flexible, Transparent, Conducting Films: Extremely High DC to Optical Conductivity Ratios. *ACS Nano* **2009**, *3* (7), 1767−1774.
(45) Scardaci, V.; Coull, R.; Lyons, P. E.; Rickard, D.; Coleman, J. N. Spray deposition of highly transparent, low-resistance networks of silver nanowires over large areas. *Small* **2011**, *7* (18), 2621−2628.
(46) Ruzicka, B.; Degiorgi, L.; Gaal, R.; Thien-Nga, L.; Bacsa, R.; Salvetat, J. P.; Forro, L. Optical and dc conductivity study of potassium-doped single-walled carbon nanotube films. *Phys. Rev. B: Condens. Matter Mater. Phys.* **2000**, *61* (4), R2468−R2471.
(47) Doherty, E. M.; De, S.; Lyons, P. E.; Shmeliov, A.; Nirmalraj, P. N.; Scardaci, V.; Joimel, J.; Blau, W. J.; Boland, J. J.; Coleman, J. N. The spatial uniformity and electromechanical stability of transparent, conductive films of single walled nanotubes. *Carbon* **2009**, *47* (10), 2466−2473.
(48) De, S.; King, P. J.; Lotya, M.; O'Neill, A.; Doherty, E. M.; Hernandez, Y.; Duesberg, G. S.; Coleman, J. N. Flexible, Transparent, Conducting Films of Randomly Stacked Graphene from Surfactant-Stabilized, Oxide-Free Graphene Dispersions. *Small* **2010**, *6*, 458−464.
(49) Higgins, T. M.; McAteer, D.; Coelho, J. C. M.; Sanchez, B. M.; Gholamvand, Z.; Moriarty, G.; McEvoy, N.; Berner, N. C.; Duesberg, G. S.; Nicolosi, V.; et al. Effect of percolation on the capacitance of supercapacitor electrodes prepared from composites of manganese dioxide nanoplatelets and carbon nanotubes. *ACS Nano* **2014**, *8* (9), 9567−9579.
(50) Nardes, A. M.; Kemerink, M.; de Kok, M. M.; Vinken, E.; Maturova, K.; Janssen, R. A. J. Conductivity, work function, and environmental stability of PEDOT:PSS thin films treated with sorbitol. *Org. Electron.* **2008**, *9* (5), 727−734.
(51) Alemu, D.; Wei, H.-Y.; Ho, K.-C.; Chu, C.-W. Highly conductive PEDOT:PSS electrode by simple film treatment with methanol for ITO-free polymer solar cells. *Energy Environ. Sci.* **2012**, *5* (11), 9662−9671.
(52) Xia, Y.; Sun, K.; Ouyang, J. Solution-Processed Metallic Conducting Polymer Films as Transparent Electrode of Optoelectronic Devices. *Adv. Mater.* **2012**, *24* (18), 2436−2440.
(53) McCarthy, J. E.; Hanley, C. A.; Brennan, L. J.; Lambertini, V. G.; Gun'ko, Y. K. Fabrication of highly transparent and conducting PEDOT:PSS films using a formic acid treatment. *J. Mater. Chem. C* **2014**, *2* (4), 764−770.
(54) De, S.; Coleman, J. N. Are There Fundamental Limitations on the Sheet Resistance and Transmittance of Thin Graphene Films? *ACS Nano* **2010**, *4* (5), 2713.
(55) De, S.; King, P. J.; Lyons, P. E.; Khan, U.; Coleman, J. N. Size Effects and the Problem with Percolation in Nanostructured Transparent Conductors. *ACS Nano* **2010**, *4*, 7064−7072.
(56) Nardes, A. M.; Kemerink, M.; Janssen, R. A. J. Anisotropic hopping conduction in spin-coated PEDOT:PSS thin films. *Phys. Rev. B: Condens. Matter Mater. Phys.* **2007**, *76* (8), 085208.
(57) Bard, A. J.; Faulkner, L. R. *Electrochemical Methods: Fundamentals and Applications*, 2nd ed.; Wiley: New York, 2000.
(58) Heywang, G.; Jonas, F. Poly(alkylenedioxythiophene)s—new, very stable conducting polymers. *Adv. Mater.* **1992**, *4* (2), 116−118.
(59) Augustyn, V.; Come, J.; Lowe, M. A.; Kim, J. W.; Taberna, P.-L.; Tolbert, S. H.; Abruña, H. D.; Simon, P.; Dunn, B. High-rate electrochemical energy storage through Li+ intercalation pseudocapacitance. *Nat. Mater.* **2013**, *12* (6), 518−522.
(60) Largeot, C.; Portet, C.; Chmiola, J.; Taberna, P.-L.; Gogotsi, Y.; Simon, P. Relation between the Ion Size and Pore Size for an Electric Double-Layer Capacitor. *J. Am. Chem. Soc.* **2008**, *130* (9), 2730−2731.
(61) Lang, X.; Hirata, A.; Fujita, T.; Chen, M. Nanoporous metal/oxide hybrid electrodes for electrochemical supercapacitors. *Nat. Nanotechnol.* **2011**, *6* (4), 232−236.
(62) Toupin, M.; Brousse, T.; Belanger, D. Charge Storage Mechanism of MnO2 Electrode Used in Aqueous Electrochemical Capacitor. *Chem. Mater.* **2004**, *16*, 3184−3190.
(63) Stoller, M. D.; Ruoff, R. S. Best Practice Methods for Determining an Electrode Material's Performance for Ultracapacitors. *Energy Environ. Sci.* **2010**, *3*, 1294−1301.
(64) Lide, D. R. *CRC Handbook of Chemistry and Physics*, 89th ed.; CRC Press: Boca Raton, FL, 2008; p 2736.

DOI: 10.1021/acsami.5b03882
ACS Appl. Mater. Interfaces 2015, 7, 16495−16506